

Volcano-Shaped Scanning Probe Microscopy Probe for Combined Force-Electrogram Recordings from Excitable Cells

B. X. E. Desbiolles,* M. T. M Hannebelle, E. de Coulon, A. Bertsch, S. Rohr, G. E. Fantner, and P. Renaud

Cite This: *Nano Lett.* 2020, 20, 4520–4529

Read Online

ACCESS |

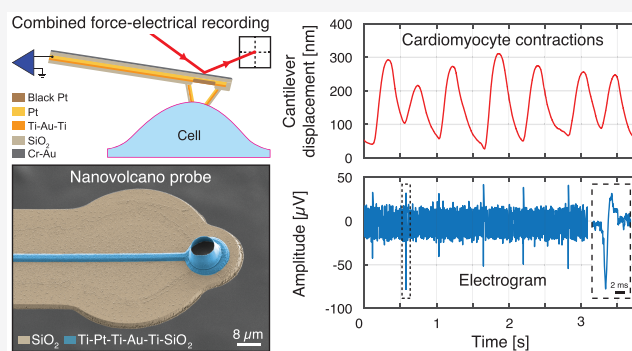
Metrics & More

Article Recommendations

Supporting Information

ABSTRACT: Atomic force microscopy based approaches have led to remarkable advances in the field of mechanobiology. However, linking the mechanical cues to biological responses requires complementary techniques capable of recording these physiological characteristics. In this study, we present an instrument for combined optical, force, and electrical measurements based on a novel type of scanning probe microscopy cantilever composed of a protruding volcano-shaped nanopatterned microelectrode (nanovolcano probe) at the tip of a suspended microcantilever. This probe enables simultaneous force and electrical recordings from single cells. Successful impedance measurements on mechanically stimulated neonatal rat cardiomyocytes *in situ* were achieved using these nanovolcano probes. Furthermore, proof of concept experiments demonstrated that extracellular field potentials (electrogram) together with contraction displacement curves could simultaneously be recorded. These features render the nanovolcano probe especially suited for mechanobiological studies aiming at linking mechanical stimuli to electrophysiological responses of single cells.

KEYWORDS: *Mechanobiology, Scanning probe microscopy, Combined force-electrophysiological recordings, Nanovolcano probe, Neonatal rat cardiomyocytes, Ion beam etching redeposition*



1. INTRODUCTION

Mechanobiology is an emerging field at the frontiers between biology and engineering that focuses on studying the role of mechanical properties of biological specimens and the effect of forces acting on those specimens in physiology.^{1–4} Over the last three decades, atomic force microscopy (AFM)⁵ has been widely used to map mechanical properties and responses of biological systems to mechanical cues.^{6–10} AFM exhibits force sensitivities in the piconewton range¹¹ with nanometer-scale lateral resolutions.¹² It is compatible with a broad range of biological samples ranging from single molecules to cells and tissues. The mechanical properties of mammalian cells were extensively studied using AFM-based approaches.^{13–20} For instance, cell differentiation^{21,22} or fibrosis²³ was shown to be dependent on the substrate stiffness. AFM was also used to study mechanical stresses during bacterial division,²⁴ turgor pressure,²⁵ and adhesion.²⁶

The key challenge in mechanobiology consists of linking functional responses of complex biological systems to mechanical stimuli.²⁷ AFM-based approaches alone are essentially blind to mechanically triggered biological responses such as changes in cellular electrophysiology and, accordingly, complementary techniques need to be developed to convey multimodal capabilities to the AFM. Presently, this is achieved

by combining AFM with optical microscopy of cells expressing or being loaded with fluorescent indicators of physiological parameters like transmembrane potentials²⁸ (e.g., voltage-sensitive dye, voltage-sensitive fluorescent proteins) or ion concentrations²⁹ (e.g., calcium indicators). As an example, cells expressing mechanosensitive ion channels can be mechanically stimulated by AFM and their electrophysiological response be monitored in real time using fluorescent calcium imaging.³⁰ Disadvantages of optical techniques include, apart from the requirement of cell manipulation and the introduction of indicators that themselves may adversely affect cellular function, phototoxicity that limits the duration of experiments.³¹ Other studies combined AFM recordings of contraction displacement of cardiomyocytes with extracellular field potential (electrograms) measurements provided by multielectrode arrays (MEA).^{32,33} Similarly, planar patch-clamp devices were used to record transmembrane potentials

Received: March 26, 2020

Revised: May 19, 2020

Published: May 19, 2020



of mechanically stimulated cells.^{34,35} Even though direct recordings of electrical activities were achieved, the limitation of these techniques mainly consist in their complexity and the lack of freedom when selecting a specific cell, because that cell has to be located exactly on top of a given microelectrode. To overcome these challenges, Ossola et al. used the FluidFM probe^{36,37} as a force-controlled nanopipette to simultaneously record force and ion channel activities in a whole-cell configuration, therefore pioneering the field of AFM-based force-controlled electrophysiology.³⁸ In this study, the electrical access to the cell was granted via an embedded microfluidic channel filled with saline solution that connected the tip opening to the recording system. Depending on the experimental question asked, this methodology has the disadvantage of wash-out of intracellular small molecules thereby compromising, for example, the integrity of the second messenger signaling cascade.³⁹ Moreover, a fluidic access to the cell significantly complicates the experimental setup as fluidic connections and pressure controllers are needed. Additionally, the embedded microchannel significantly limits the minimal cantilever thickness achievable, therefore limiting the bandwidth and the sensitivity during force measurements.

Cells are constantly interacting with each other and with their environment through chemical, mechanical, and electrical factors. The latter include mechanical forces, cellular stiffness, electrical potentials, and ion currents that determine the cell behavior. Here, we propose a new fluidic-free instrument that combines within a single probe measurement capabilities for optical, electrical, and mechanical factors determining cell functions. Central to the device is a novel type of probe for scanning probe microscopy (SPM) consisting of a protruding three-dimensional (3D) volcano-shaped microelectrode at its apex that enables fluidic-free combined force and electrophysiological recordings from single cells or tissues. The device is termed “nanovolcano probe” as it integrates our recently developed nanovolcano electrode⁴⁰ at the tip of an AFM cantilever.

Force and impedance were concurrently measured when engaging onto neonatal rat cardiomyocytes to confirm the proper functioning of the probe in a conventional AFM setup. Thereafter, the nanovolcano probe was used to investigate whether it could be used to record simultaneously mechanical and electrophysiological activity from single cells. Successful recording of electrograms together with cardiomyocyte contraction displacements demonstrated that the nanovolcano probe enables combined force-electrogram recordings. These findings render the nanovolcano probe particularly suitable for mechanobiological studies aiming at linking electrophysiological responses with mechanical stimuli at the single-cell level.

2. RESULTS

2.1. Microfabrication. The nanovolcano probe concept and design are summarized in Figure 1A. The inner surface of the 8 μm -wide nanovolcano consists of a large electrodeposited platinum-black electrode that minimizes the access impedance to the cell. The outside of the 6 μm high structure is covered with a 20 nm thick insulating SiO_2 layer that prevents current leaks from the electrode. Furthermore, a 5–10 nm thick gold nanoring stacked in-between two Ti layers and functionalized with self-assembled monolayers of alkanethiols forms the site of contact with the cell membrane and is thought to optimize the cell–electrode interface.^{41–45} The microelectrode is attached to a 2.2 μm thick SiO_2 cantilever that is coated on

the backside with a 50 nm thick Cr–Au reflective layer allowing for conventional optical beam deflection measurement in an AFM.⁴⁶

As illustrated in Figure 1B, conventional ion beam etching was used to pattern 3 μm wide conductive tracks on a Si substrate covered with a 2 μm thick layer of thermally grown SiO_2 that was subsequently insulated with 200 nm of sputtered SiO_2 . The nanovolcano was then manufactured at the tip of the Ti–Pt–Ti–Au–Ti– SiO_2 pattern by ion beam etching redeposition.^{40,47} To this end, openings with a diameter of 8 μm were patterned into a 6 μm thick negative photoresist layer. During ion beam etching, a part of the etched material from the substrate was redeposited onto the photoresist sidewalls, thereby creating the multilayered nanovolcano wall after resist stripping by O_2 plasma. The SiO_2 cantilever was then defined with a wider circular shape close to the tip to maximize the laser reflection and released by reactive ion etching (RIE). Because of the compressive stress accumulated in the SiO_2 layer during thermal growth, the released cantilever bent in the opposite direction from the substrate. In a final fabrication step, stressed layers of Cr–Au (50–50 nm) were evaporated onto the backside of the cantilever to compensate for their bending and to render them reflective.

Scanning electron microscope (SEM) images of the finalized nanovolcano probe are shown in Figure 1C–E. As illustrated by Figure 1C,D, the SiO_2 cantilever dimensions were chosen such as to ensure a stiffness comparable to cells (for the nanovolcano probe: $k_{\text{Measured}} = 0.45 \text{ N/m}$). The nanovolcano electrode placed at the tip of the cantilever was fabricated with a relatively large diameter to ensure a low electrode–electrolyte impedance while permitting a sufficient lateral resolution to perform experiments at the single-cell level. The height of the nanovolcano guaranteed that the nanovolcano touched the sample first during AFM manipulation. The inset in Figure 1E shows the 7 nm thick gold nanoring flanked by two titanium layers in the middle of the 70 nm thick multilayered nanovolcano wall. A complete characterization of the nanovolcano wall cross-section by transmission electron microscopy combined with energy dispersive X-ray spectroscopy can be found in our previous work.⁴⁰

The nanovolcano probe was interfaced to a custom-made AFM holder (see Supporting Information, Section 1) and platinum-black was locally electrodeposited into the nanovolcano to decrease its electrode–electrolyte impedance. A complete electrochemical characterization of the nanovolcano probe is provided in Supporting Information, Section 2.

2.2. Force and Electrical Measurements on Neonatal Rat Cardiomyocytes. The nanovolcano probe was mounted on a custom-made setup composed of a tip-scanning AFM mounted above an optical inverted microscope and a custom sample holder to keep the biological sample in physiological conditions (see Materials and Methods). Experiments with neonatal rat cardiomyocytes were performed to validate that both force and impedance signals can be recorded simultaneously by the nanovolcano probe.

Cardiomyocytes were cultured at low density for 48 h prior to the experiment. During experiments, the cantilever position and deflection were recorded while the nanovolcano probe was repeatedly brought in contact with a cell of interest followed by pulling away using the AFM piezoelectric actuator. A typical result of such an experiment is shown in Figure 2A: the probe was initially lowered toward the cell by $\sim 11 \mu\text{m}$ while applying a maximal force of 772 nN before being withdrawn again at $t =$

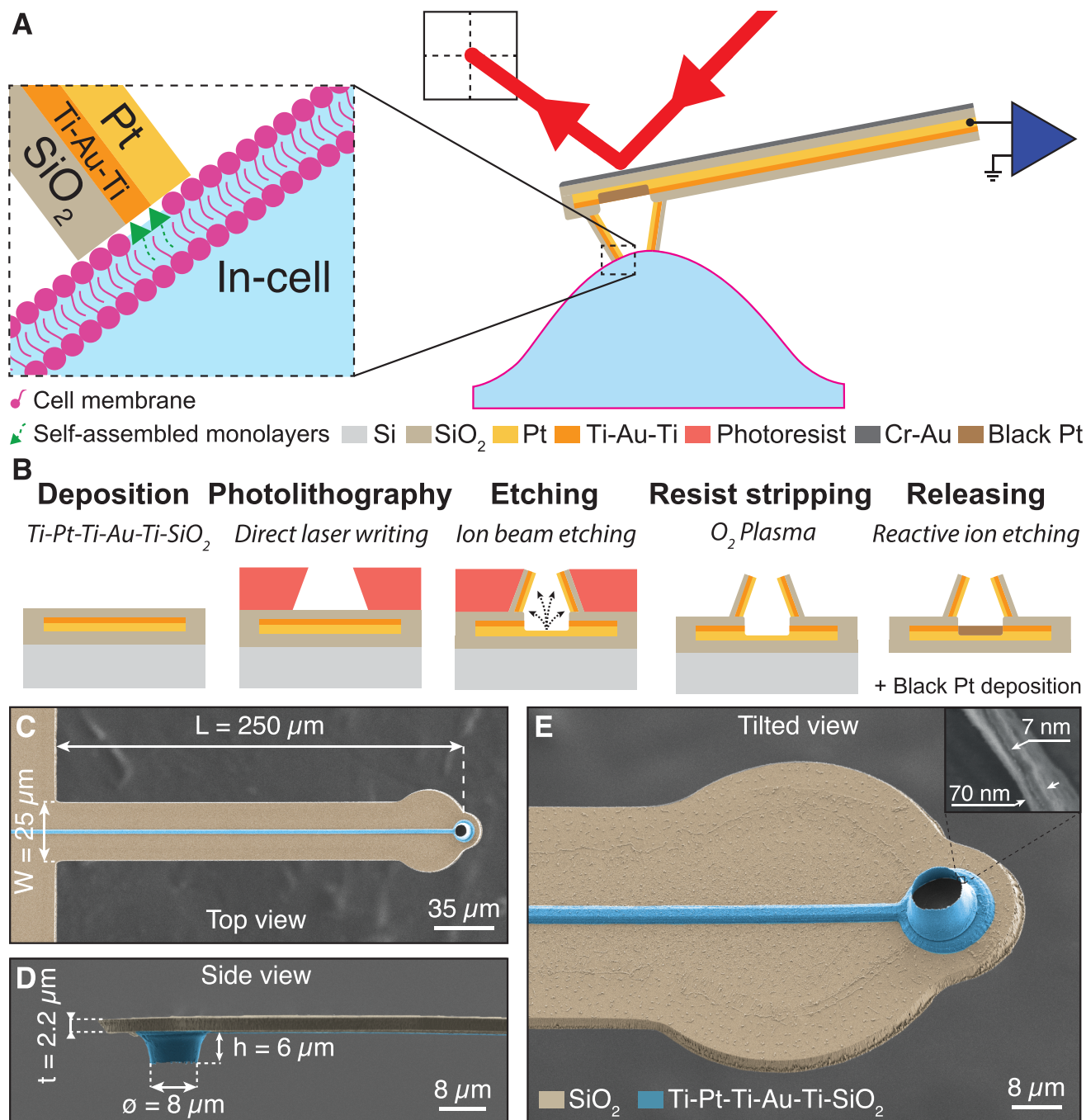


Figure 1. Concept and microfabrication of the nanovolcano probe. (A) Schematic drawing showing the nanovolcano probe in contact with a cell. The cantilever deflection as well as the electrical signal from the nanovolcano are measured simultaneously. The inset shows the cell–electrode interface in detail. (B) Microfabrication process used to manufacture the nanovolcano probe. Insulated metallic tracks are patterned onto a 2 μm thick SiO₂ layer covering the Si substrate. During ion beam etching, the material etched from the substrate is redeposited on the photoresist sidewalls therefore forming the nanovolcano after resist stripping. The SiO₂ cantilever is subsequently defined and released by reactive ion etching. (C–E) SEM images showing top view, side view, and tilted view (angle of 30°) of the nanovolcano probe. The volcano electrode structure and the conductive tracks are colored in blue.

0.25 s. The maximally applied force is 3 orders of magnitude larger than the force usually used as a set point for nondestructive AFM imaging (a few hundred pN). However, because the contact area between the nanovolcano rim and the cell under investigation is about 3 orders of magnitude larger than the contact area of a pyramidal cantilever tip, local strain, and stress applied to the cell are below the cell damage

threshold for the nanovolcano measurements as well. The ramp curve depicting the force–position relation (Figure 2B) shows a typical smooth increase of the force between 7 and 11 μm indicating indentation of the cell by the nanovolcano. The hysteresis visible in the force curve is due to mechanical energy dissipated by the cell, whereas the step during withdrawing highlights the detachment of the cantilever from the cell.

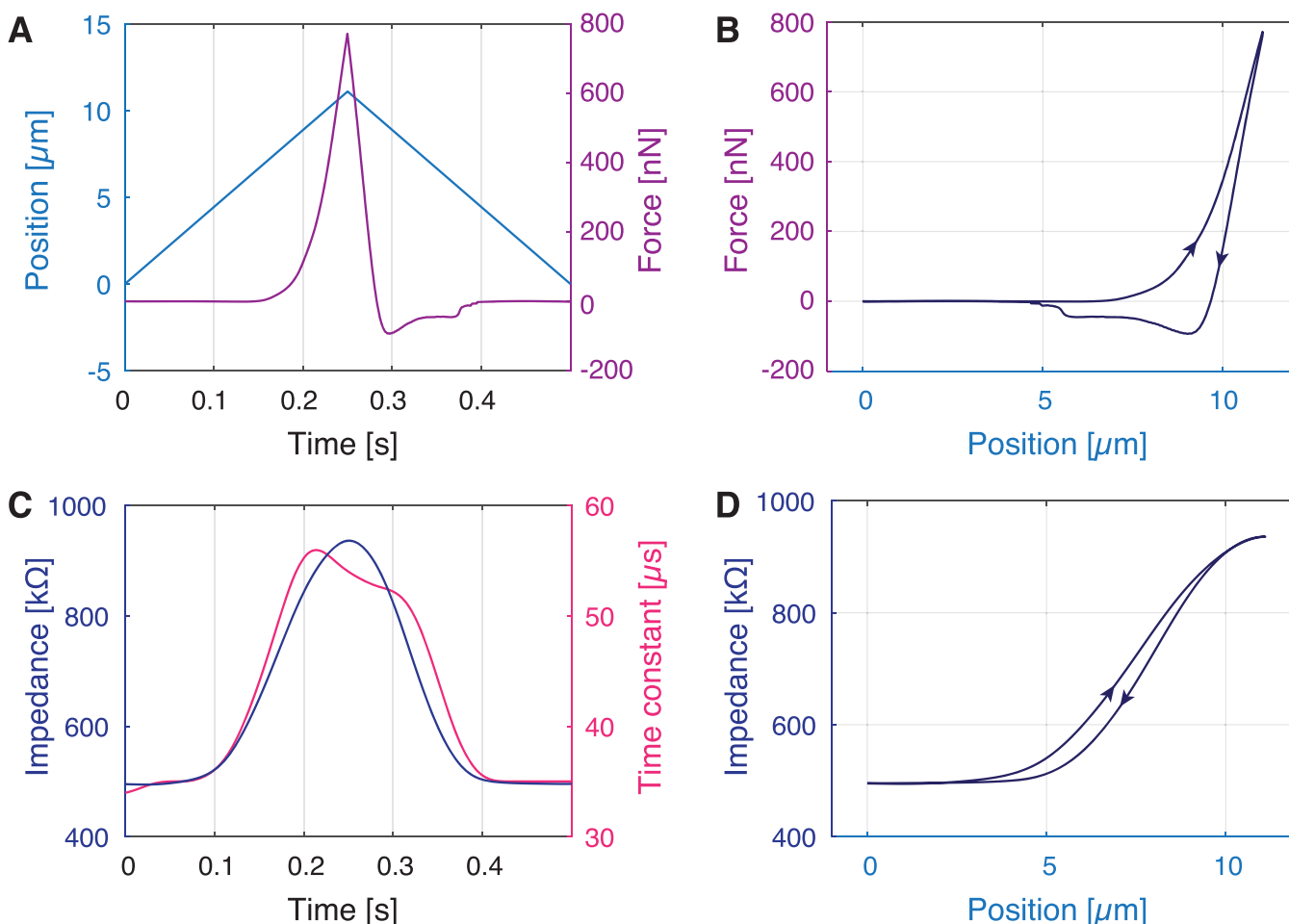


Figure 2. Force and electrical measurements on neonatal rat cardiomyocytes. (A) Evolution of the nanovolcano cantilever position along the z -axis (left axis, light blue) and the resulting force applied to the cell (right axis, purple) with time. The first contact with the cell was initiated at $t \approx 0.15$ s and position $\sim 7 \mu\text{m}$ (maximum force = 772 nN). (B) Ramp curve showing the force–position relationship. (C) Evolution of the nanovolcano probe impedance (left axis, dark blue) and time constant (right axis, magenta) with time, measured by pulsed amperometry. (D) Ramp curve showing the impedance–position relationship.

Simultaneous with the force measurements, square wave amperometry was performed through the nanovolcano probe to observe the impedance variation when engaging onto a cell. A 5 mV square wave oscillating at 20 Hz was applied between the nanovolcano and a counter electrode located in the bath while measuring the resulting current. Capacitive current peak amplitudes and current pulse time constants were extracted and plotted in Figure 2C as the tip approached the cell and then was withdrawn again. Both the “high frequency impedance” and the time constants significantly increased when the probe came close to the cell. Impedance increased to 189% and time constants to 160%. No variations of the resistive current at low frequency were observed. In Supporting Information, Section 2, an electrical equivalent circuit of the cell–electrode interface is presented that illustrates the increase of the impedance and time constant as the probe approached the cell. Figure 2D shows the variation of impedance with respect to the cantilever position. A significant increase of high-frequency impedance can be noted for cantilever displacements larger than 3 μm that saturates at 10.5 μm . Force-controlled impedance measurements conducted on nonbeating human embryonic kidney (HEK) cells showed similar behaviors compared to cardiomyocytes, therefore suggesting that spontaneous contractions did not

significantly influence the impedance measurements. Amperometric measurements allow for an earlier cell detection compared to force recording. Forces in the nanonewtons range were applied and currents with <10 pA amplitude were measured. This experiment was successfully repeated on seven different HEK cells and seven primary rat cardiomyocytes with two different cantilevers. Experimental results are summarized in Supporting Information, Subsection 3.1.

2.3. Recording of Cardiomyocyte Contraction Displacements Using the Nanovolcano Probe. Following the basic characterization of the nanovolcano probe, we tested its suitability for performing measurements of contraction displacements from spontaneously active primary neonatal rat ventricular cardiomyocytes. Cardiomyocytes were cultured at low density for 48–72 h prior to the electrophysiological recordings. The time-lapse images in Figure 3A show one contraction of a spontaneously active cell studied with the nanovolcano probe maintained at a constant height. The blue pixels illustrate the variation of intensity compared to the previous frame and therefore highlight the contraction-related movement of the cell. At t_0 , the cardiomyocyte is quiescent. It initiates its contraction at $t_{1,2}$, stays contracted during $t_{3,4}$ before relaxing again at t_{5-9} . The bottom panel in Figure 3A represents the sum of the derivative for every pixel from the

video in the region of interest presented in the top panel. This measure is conventionally used to quantify cardiomyocyte contractions^{48,49} and serves as visual control for the nanovolcano measurements.

Cantilever displacements recorded in parallel are shown in Figure 3B (top panel). The first contraction (corresponding to the time-lapse data) has an amplitude of 367 nm and a duration (at 10% of the amplitude) of 646 ms. Similarly, the second contraction had an amplitude of 422 nm and displayed a duration of 614 ms. The panel below depicts the corresponding derivatives (absolute values). For both activations, contraction rates amounted to 2.9 and 3.5 $\mu\text{m/s}$, respectively. Relaxation was slower and amounted to 1.5 and 1.7 $\mu\text{m/s}$, respectively. The absolute derivatives of the cantilever displacement and those derived from the video data reliably matched. Additional contraction displacement characteristics measured from five different primary rat cardiomyocytes using the nanovolcano probe are presented in Supporting Information, Subsection 3.2.

2.4. Simultaneous Recording of Contraction Displacements and Electrogram from Cardiomyocytes Using the Nanovolcano Probe. Neonatal rat ventricular cardiomyocytes were also used to investigate the possibility of recording contraction displacement together with electrophysiological activity using the nanovolcano probe. As demonstrated in Figure 4, both contraction displacements (cf. Figure 4A) and electrograms (cf. Figure 4B) could simultaneously be recorded by the nanovolcano probe. Electrograms showed typical biphasic shapes and displayed amplitudes ranging from -38 to -75 μV that slightly preceded contraction. During a 25 s long recording session, contraction amplitudes of 250 ± 35 nm with a duration at 50% amplitudes of 225 ± 35 ms (average \pm standard deviation) were observed together with electrograms showing downstroke amplitudes of 47 ± 9 μV ($N = 49$). Electrograms recorded from a second cell with the same probe produced similar results (cf. Supporting Information, Subsection 3.3). This demonstrates the possibility to perform successive electrogram recordings at different locations using a single probe.

3. DISCUSSION

The novel SPM probe presented in this study enables direct combined force and electrical signal recordings by placing a 3D microelectrode at the tip of an AFM cantilever. The protruding electrode at the cantilever tip combines several technological advances in a single structure: (1) the platinum-black-coated nanovolcano interior ensures a relatively low electrode impedance and, hence, optimizes signal-to-noise ratios (see Supporting Information, Section 2.1); (2) the electrically insulating nanovolcano walls prevent current leakage from the electrode which contribute to the robustness of the cell–electrode interface robustness.

The 3D multimaterial nanopatterned microelectrode was manufactured following a reliable and scalable nonconventional four-step fabrication process based on ion beam etching redeposition that was completed with the patterning and release of the cantilever by conventional reactive ion etching techniques. All manufacturing steps used to produce both the nanopatterned electrode and the cantilever are compatible with complementary metal oxide semiconductor (CMOS) technologies. Accordingly, it is feasible to integrate CMOS amplifiers on the nanovolcano probes in the future to minimize electrical signal attenuation and noise. In contrast to previous

technologies using FIB milling,^{38,50} the fabrication process is simple, scalable, and leads to homogeneous structures at the wafer scale (>250 chips per wafer). Compared to regular nanovolcano arrays,⁴⁰ the photoresist layer used to manufacture the 3D microelectrode presented in this study is thicker which results in a wider undercut after development. As a consequence, the redeposited materials composing the nanovolcano wall are electrically insulated from the electrode area (cf. Figure 1B) thereby preventing the gold nanoring to be coated during platinum-black electrodeposition.

Compared to conventional conductive AFM tips, nanovolcano probes show the distinct advantage of being insulated up to the very end of the tip, allowing for a confined measurement with minimal current leaks. Furthermore, the volcano geometry enables low access impedance in physiological saline solutions compared to conductive AFM tips and therefore permits electrophysiological recordings.

Simultaneous force and impedance recordings on neonatal rat cardiomyocytes confirmed that pulsed amperometry could be used to gauge the engaging process and allows for gentle engaging on soft biological samples. As already reported in the literature, the probing depth of a microelectrode is mainly influenced by its spreading resistance and proportional to its radius.⁵¹ For this reason, cells were detected by impedance measurements ~ 4 μm (approximate microelectrode radius) prior to mechanical contact. Presently, the lateral resolution achievable with the nanovolcano probe is limited by the 8 μm in diameter protruding electrode. The relatively large electrode area is necessary to decrease the electrode impedance at the electrode–electrolyte interface and therefore to permit electrical measurements. Prospectively, platinum black could be substituted by lower impedance materials (e.g., PEDOT:PSS) to potentially achieve similar access resistances for smaller electrode diameters, thus improving the lateral resolution.

These experiments demonstrated that the nanovolcano probe was suited to map the impedance properties of mechanically stimulated cells at the single-cell level, hence providing opportunities in the field of mechanobiology.

When performing experiments with primary neonatal rat ventricular cardiomyocytes, their morphology and contractility did not change during the duration of the experiments. For the first time, electrograms together with contraction displacements were successfully recorded using a single probe and were confirmed by simultaneous optical recordings. Positive monophasic cantilever displacements with an amplitude and duration similar to the ones observed with conventional probes were reported.³² Simultaneously, biphasic voltage pulses corresponding to electrograms showed shapes, durations, and amplitudes consistent with extracellular activities recorded with standard MEAs.⁵² Even though amplitudes close to 1 mV are commonly reported in the literature for cardiomyocyte monolayers, recording performed on single cardiomyocyte with conventional MEAs showed similarly low amplitudes (<100 μV).⁵³

The nanovolcano probe permits combined force-electrogram measurements within a single probe and therefore is an alternative to the AFM-MEA system that has, besides a reduction of system complexity, the added advantage of permitting the free selection of cells of interest. In comparison to FluidFM technology, no microfluidic channels were needed to transmit the electrical signal from the tip to the recording system, therefore bypassing the high fluid resistance and

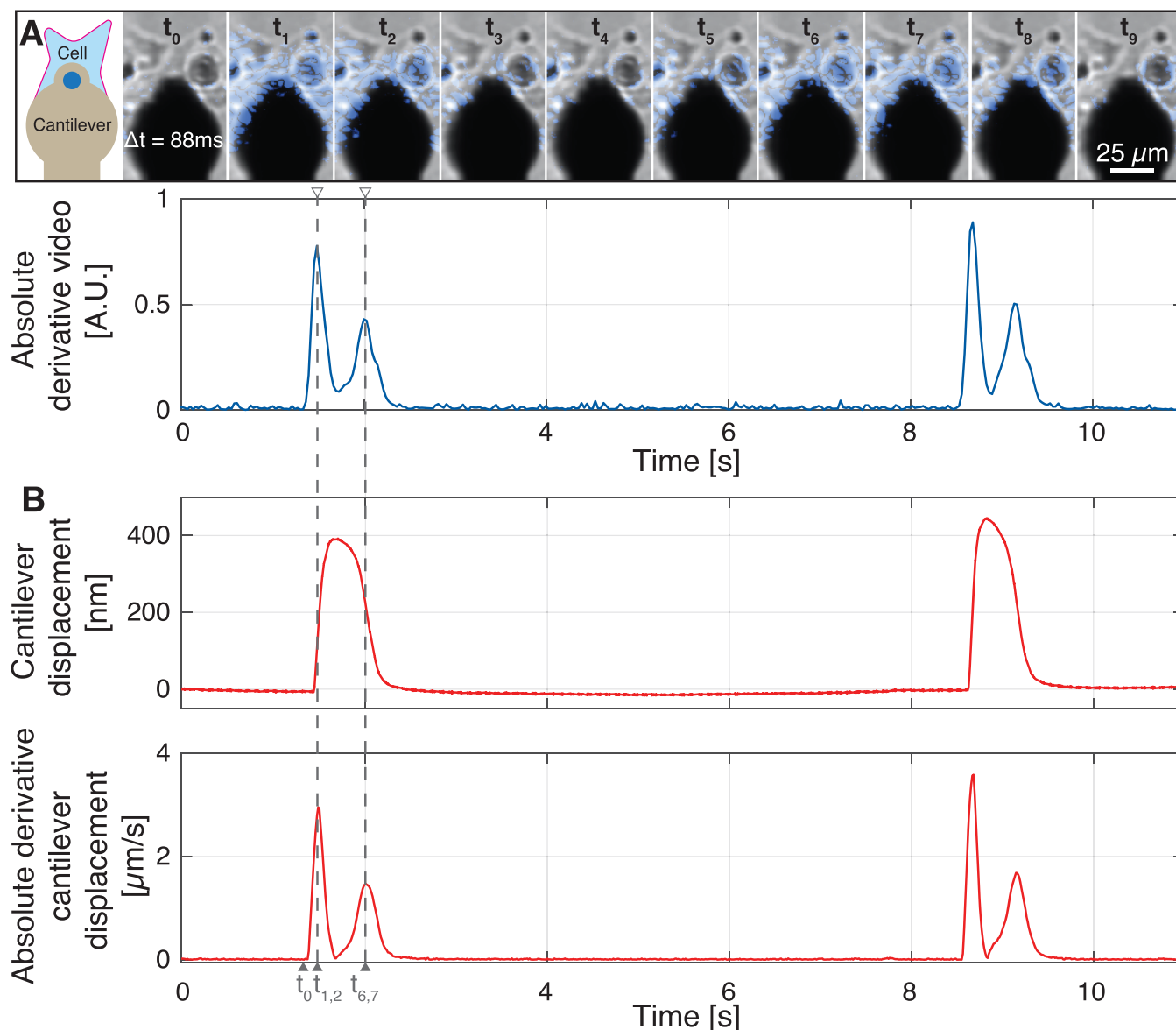


Figure 3. Recording of contraction displacements from primary rat cardiomyocytes. (A) Upper panel: Schematic drawing (left) and series of time lapse images showing the nanovolcano probe engaged on a beating cardiomyocyte (right). Pixels showing intensity variations compared to the previous frame are highlighted in blue and indicate cardiomyocyte contraction.^{48,49} Lower panel: Temporal evolution of the sum of the derivatives of every pixels for the entire area depicted in the upper panel. (B) Cantilever displacement (top panel) and its absolute derivative (bottom panel) from the same cardiomyocyte. The first contraction starts at t_0 and corresponds to the time-lapse images presented in (A). The cantilever displacement absolute derivative matches the absolute derivative of the video signal.

simplifying the experimental system.³⁸ Compared to the recently developed ultrasmall nanowire transistor probes (U-NWFET) enabling intracellular recording of action potentials from individual cells,⁵⁴ the nanovolcano system is limited to recording electrograms only but has the advantage of permitting simultaneous force recording.

Future developments of the nanovolcano probe should focus on permitting combined force and intracellular electrophysiological recordings such as action potentials or ion-channel activity. This might be challenging as, compared to extracellular recording, a high seal resistance is essential in intracellular electrophysiology to maintain the punctured cell activity and enable high quality recordings. In this study, the seal resistance was estimated to be much lower than the nanovolcano probe access resistance ($R_{\text{seal}} < 309 \text{ M}\Omega$, see [Supporting Information](#), Section 2.2). The nanometer-wide

alkanethiol's nanopattern hypothesized to strengthen the cell–electrode interface was seemingly not sufficient to provide the gigaseal required to perform decent intracellular electrophysiology. Nevertheless, a systematic investigation of the nanopattern contribution to the seal formation could be performed with diverse types of self-assembled monolayers, not only based on alkane chains but also on positively charged molecules (e.g., polyamine) or proteins (glutaraldehyde). On the other hand, a chemical–mechanical polishing step of the nanovolcano tip could be added in the microfabrication process to significantly reduce its roughness, potentially improving the interface strength. In this context, the nanovolcano probe is certainly of interest to characterize the cell–electrode interface electrical properties by in situ impedance spectroscopy.

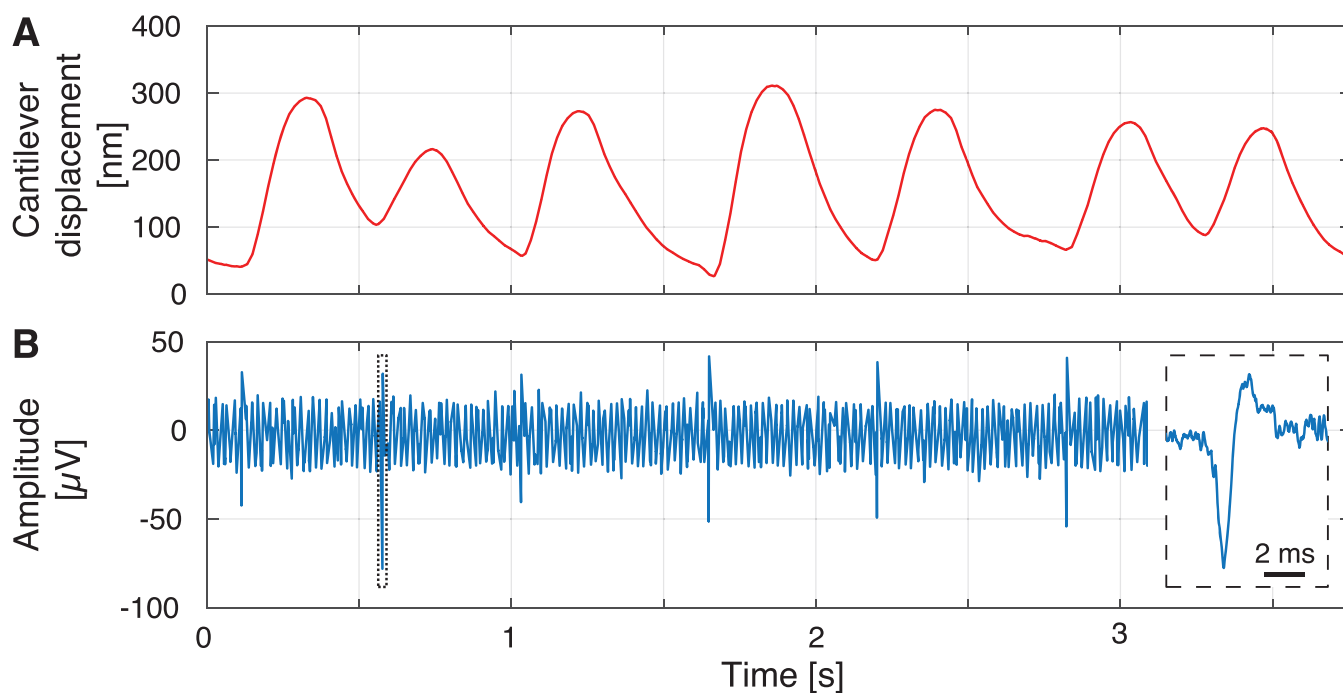


Figure 4. Simultaneous recording of cardiomyocyte contraction displacements electrograms. (A) Cantilever displacement simultaneously recorded with (B) electrograms from a spontaneously active cardiomyocyte using the nanovolcano probe. The insert presents an expanded view of the region of the electrogram framed with dashed lines.

4. CONCLUSION

In this work, we present an instrument for combined optical, force, and electrical measurements using a novel type of SPM probe composed of a nanopatterned volcano-shaped protruding electrode. Parallel mechanical, optical, and electrical measurements of single cells were acquired thereby presenting a new approach for integrated mechano-electrical investigations.

The protruding microelectrode is electrically insulated to prevent current leaks at the cell–electrode interface. Additionally, a platinum-black coating of the large electrode area results in a relatively low impedance at the electrode–electrolyte interface. The complex 3D multimaterial microstructure was successfully manufactured at the tip of a suspended cantilever, exploiting a straightforward process that is reliable at the wafer scale. It combines a nonconventional redeposition processes occurring during ion beam etching with standard microfabrication techniques.

Experiments with neonatal rat cardiomyocytes demonstrate that the nanovolcano probe enables *in situ* impedance recordings of mechanically stimulated cells with conventional liquid AFM setups. Proof of principle experiments confirm that a combined measurement of force and electrical signals can be achieved with the presented probe. Electrograms and contraction displacements from spontaneously active cardiomyocyte were simultaneously recorded with similar characteristics to the one measured with conventional methods.

These features render the nanovolcano probe particularly suitable for mechanobiological studies aimed at linking functional electrophysiological single-cell responses with mechanical stimuli.

5. MATERIALS AND METHODS

5.1. Microfabrication. A 380 μm thick double-side polished silicon wafer (100 mm in diameter) coated with 2 μm of SiO_2 obtained by wet thermal oxidation was covered by successive evaporations of Ti–Pt–Ti–Au–Ti (10–250–100–100–100 nm) using an EVA 760 e-beam evaporator (Alliance Concept, France). Electrically conductive tracks were patterned in a 750 nm thick layer of AZ ECI 3007 positive photoresist layer (MicroChemicals, Germany) spin coated with a Rite Track 88 series automatic coater (Rite Track, U.S.A.), exposed with an i-line VPG 200 direct laser writer (Heidelberg, Germany) at a dose of 93 mJ/cm^2 and developed for 36 s in an AZ 726 MIF commercial developer (MicroChemicals) using a Rite Track 88 series automatic developer (Rite Track). Thereafter, a 2 min reflow at 120 $^\circ\text{C}$ was performed on a Sawatec HP200 hot plate (Sawatec, Switzerland) prior to etching the substrate positioned at an angle of incidence of -35° with respect to the ion beam generated in an IBE 350 ion beam etcher (Veeco, U.S.A.) for 9 min 30 s. The photoresist was stripped in a 500 W O_2 plasma (O_2 flow 400 mL/min) for 7 min created by a TePla 300 microwave plasma system (PVA TePla, Germany). The conductive tracks were subsequently insulated by 200 nm of SiO_2 sputtered with a Spider 600 sputter-coater (Pfeiffer Vacuum, France).

A monolayer of hexamethyldisilazane (HMDS) was deposited on the topmost SiO_2 layer using a primer hot plate VB20 (ATMsse, Germany) before spin coating a 6 μm thick layer of negative photoresist AZ nLoF 2070 (MicroChemicals) using an OPTIspin SB20 manual coater (ATMsse) rotating at 3500 rpm. Eight micrometer diameter openings were patterned in the photoresist layer using an i-line VPG200 direct laser writer (Heidelberg) operating at a dose of 105 mJ/cm^2 . After a postexposure bake at 110 $^\circ\text{C}$ with a 50 μm proximity gap for 75 s, the wafer was developed for 91 s using

an AZ 726 MIF developer (MicroChemicals) dispensed using an EVG150 automatic coater/developer (EVG, Austria). The sample was then bombarded with Ar^+ ions for 15 min at an angle of incidence of 0° using an IBE350 ion beam etcher (Veeco). During this step, materials from the substrate were etched and redeposited on the photoresist sidewalls. The photoresist was finally stripped by O_2 plasma (10 min, 500 W, O_2 flow 400 mL/min) in a Tepla 300 microwave plasma system (PVA TePla), letting the nanovolcanoes protrude from the insulated tracks.

Both the cantilever and chip body were then patterned into a 15 μm thick AZ 40xT photoresist layer (MicroChemicals) coated with an ACS200 gen 3 automatic coater-developer (Süss, Germany), exposed with an i-line VPG200 direct laser writer (Heidelberg) at a dose of 93 mJ/cm^2 , and developed in an AZ 726 MIF developer (MicroChemicals) for 80 s using an ACS200 gen 3 automatic coater-developer (Süss). Following an overnight bake at 85°C in a Heraeus T6060 oven (Heraeus, Germany), the cantilever shape was transferred into the 2.2 μm thick SiO_2 layer by a 7 min long reactive ion etching process ($\text{He}/\text{H}_2/\text{C}_4\text{F}_8$ based chemistry) performed using a SPTS APS dielectric etcher (SPTS, United Kingdom). The cantilever and chip body outlines were subsequently etched throughout the 380 μm thick Si wafer by Bosch processing in an AMS 200 dry etcher (AMS, Austria) until reaching the 2 μm thick backside Al etching stop layer deposited beforehand with an EVA760 e-beam evaporator (Alliance Concept). Finally, the SiO_2 cantilever was released by Si isotropic dry etching performed in an AMS 200 reactive ion etcher (AMS). The photoresist was then removed by O_2 plasma (10 min, 500 W, O_2 flow 400 mL/min) performed in a TePla 300 microwave plasma system (TePla), followed by a 15 min long piranha etch ($\text{H}_2\text{SO}_4/\text{H}_2\text{O}_2$, 3:1) to remove both dry etching residues as well as the backside Al membrane.

The 2.2 μm thick SiO_2 handlers connecting the chips to the substrate were manually removed to place the cantilevers upside down in an EVA760 e-beam evaporator (Alliance Concept) and to coat their backside with 50 nm thick layers of Cr and Au.

5.2. Interfacing. The nanovolcano probe was mechanically assembled on a custom-made PCB using a H20E epoxy cured for 3 h at 80°C (Epoxy Technology, U.S.A.). The PCB was then mounted onto a custom-made AFM holder prior to wire-bonding the chip contact pad (electrically connected to the nanovolcano) with the PCB gold-coated pad (linked to a standard U. FL coaxial cable) using a HB05 wedge and ball bonder (TPT, Germany). The chip-PCB interface was electrically insulated using a $\text{H70} \times 10^{-2}$ glob top epoxy (Epoxy Technology) that was dispensed manually and cured at 80°C for 1 h 30 min. Optical images of the interface are presented in [Supporting Information](#), Section 1.

5.3. Electrodeposition of Platinum-Black. Platinum-black was locally deposited into nanovolcanoes by pulsed potentiostatic deposition as described before.⁵⁵ Briefly, the nanovolcanoes were electrochemically treated by varying the electrode potential from -0.2 to $+1.2$ V vs Ag/AgCl (scan rate of 100 mV/s) for 20 cycles in a 0.5 M H_2SO_4 solution. Subsequently, the microelectrodes were immersed into a solution of hexachloroplatinic acid (17.5 mmol/L, 262587, Sigma) and lead(II) acetate trihydrate (0.03 mmol/L, 467863-50G, Sigma) prior to applying -700 mV voltage pulses with respect to the open circuit potential (V_{OCP}) for an

overall duration of 45 s ($t_{\text{on}} = 0.2$ s, $t_{\text{off}} = 0.4$ s, number of pulses = 225).

5.4. Isolation and Culture of Primary Rat Cardiomyocytes. Primary neonatal rat (Wistar, 1 day old) ventricular cardiomyocytes were isolated using established procedures in compliance with federal guidelines for animal experimentation under license BE27/17 of the Bernese Veterinary Department. The resulting cell suspension was centrifuged at 1000 rpm for 5 min, resuspended in DMEM (41965-039, Gibco) containing 10% fetal bovine serum (16140071, ThermoFisher Scientific) and 1% penicillin/streptomycin, and seeded in 6 cm diameter Petri dishes at a density of ~ 350 cells/ mm^2 . Cells were incubated at 37°C in an atmosphere containing 5% CO_2 . The cell medium was renewed every 24 h. Experiments were conducted 48–72 h postseeding. At this time, the cellular electrophysiology of cardiomyocytes has recovered from the isolation process and overgrowth with noncardiomyocytes such as myofibroblasts is still moderate.

5.5. Device Functionalization. The nanovolcano probes were sterilized for 30 s with O_2 plasma (100 W, 650 mTorr; Diener Electronic, Germany) prior to being immersed for 1 h in a 20 mM hexanethiol solution in pure ethanol for self-assembled monolayer formation. After ethanol rinsing, the probes were thoroughly rinsed in sterile deionized water.

5.6. Combined AFM-Optical-Electrical Setup and Recordings. A detailed description of the system combining AFM, optical, and electrical recordings is presented in [Supporting Information](#), Section 1.

In short, the combined AFM-optical setup is a custom system⁵⁶ associating a tip-scanning AFM (Dimension Icon, Bruker, Germany) and an optical microscope (IX73 or IX81, Olympus, Japan) equipped with a 20 \times objective and a camera (ixon Ultra 897, Oxford Instruments, United Kingdom). The camera was used in frame transfer mode with a 20 Hz acquisition rate. The AFM was used in contact mode without (constant height mode) or with feedback enabled (constant deflection mode). Contraction displacement curves were established by converting image data into height and deflection as a function of time. Data were recorded while imaging with a scan size of 0 nm, a scan rate of about 40 Hz and 1024 samples per line, which corresponds to a sampling rate of about 80 kHz. The images were preprocessed using gwyddion,⁵⁷ before further processing with a custom Matlab script to convert the “trace” and “retrace” AFM images into height and deflection as a function of time.

Two different nanovolcano probes were used to collect the data presented in this study. Impedance measurements were performed with probes 1 and 2. Probe 2 was subsequently cleaned by O_2 plasma (100W, 650 mTorr, 30 s; Diener Electronic), inspected by SEM, functionalized, and reused to record electrophysiological signals from cardiomyocytes.

5.7. Electrophysiology. Electrophysiological recordings were performed at room temperature on preparations kept in Hank's balanced salt solution supplemented with 10 mmol/L Hepes (pH 7.2). An Axopatch 200B microelectrode amplifier together with a CV 203 BU headstage (Molecular Devices, U.S.A.) were used to perform pulsed amperometry and to record electrograms from cardiomyocytes (bandwidth, 0–100 kHz). The analog to digital conversion was performed by a Powerlab 4/25 acquisition card (AD Instruments, Australia) at a sampling frequency of 200 kS/s. Extracellular signals were post processed with a Butterworth bandpass filter (100–500 Hz).

■ ASSOCIATED CONTENT

Supporting Information

The Supporting Information is available free of charge at <https://pubs.acs.org/doi/10.1021/acs.nanolett.0c01319>.

Detailed information regarding the electrical and mechanical chip interfacing with its custom-made AFM holder, optical-AFM custom-made system, experimental characterization of the electrode–electrolyte interface, cell–electrode interface modeling, long-term electrochemical characterization of the nanovolcano probe, and additional experimental data (PDF)

■ AUTHOR INFORMATION

Corresponding Author

B. X. E. Desbiolles – Laboratory of Microsystems LMIS4, Ecole Polytechnique Fédérale de Lausanne, Lausanne 1015, Switzerland; orcid.org/0000-0001-6848-3289; Email: benoit.desbiolles@epfl.ch

Authors

M. T. M Hannebelle – Laboratory of Bio- and Nano-Instrumentation, Ecole Polytechnique Fédérale de Lausanne, Lausanne 1015, Switzerland
E. de Coulon – Laboratory of Cellular Optics II, Department of Physiology, University of Bern, Bern 3012, Switzerland
A. Bertsch – Laboratory of Microsystems LMIS4, Ecole Polytechnique Fédérale de Lausanne, Lausanne 1015, Switzerland
S. Rohr – Laboratory of Cellular Optics II, Department of Physiology, University of Bern, Bern 3012, Switzerland
G. E. Fantner – Laboratory of Bio- and Nano-Instrumentation, Ecole Polytechnique Fédérale de Lausanne, Lausanne 1015, Switzerland
P. Renaud – Laboratory of Microsystems LMIS4, Ecole Polytechnique Fédérale de Lausanne, Lausanne 1015, Switzerland

Complete contact information is available at: <https://pubs.acs.org/doi/10.1021/acs.nanolett.0c01319>

Author Contributions

P.R. and B.X.E.D. conceived the project, B.X.E.D. manufactured the nanovolcano probe in a clean room, B.X.E.D. and M.T.M.H. developed the interface, G.E.F. and M.T.M.H. provided the combined AFM-optical setup, E.d.C. and S.R. handled the cardiomyocyte isolation and B.X.E.D. the culture, M.T.M.H. and B.X.E.D. conducted the electrophysiological experiments, B.X.E.D., M.T.M.H., E.d.C., and S.R. interpreted the results, P.R., G.E.F., and A.B. supervised the technological part of the project and S.R. the biological part. All authors discussed the results and contributed to the final manuscript.

Notes

The authors declare no competing financial interest.

■ ACKNOWLEDGMENTS

This work was partially funded by the Swiss National Science Foundation (Grants 200021-175943 to P.R. and 310030_169234 to S.R.) and the H2020 - UE Framework Programme for Research & Innovation (2014-2020); ERC-2017-CoG; InCell; Project number 773091. The authors thank the EPFL Center of Micronanotechnology (CMi) staff for their outstanding support and availability. Special thanks to Dominik Ziegler (Scuba Probe Technologies LLC) for his help

with the long-term electrochemical characterization, Rodrigo de Campos Perin (EPFL) for kindly lending us the Axopatch 200B amplifier, Mathieu Aberle (EPFL) for his preliminary contribution, and Regula Flückiger Labrada (UNIBE) for her cell culture work.

■ REFERENCES

- (1) Hoffman, B. D.; Grashoff, C.; Schwartz, M. A. Dynamic molecular processes mediate cellular mechanotransduction. *Nature* **2011**, *475*, 316–323.
- (2) Howard, J.; Grill, S. W.; Bois, J. S. Turing's next steps: The mechanochemical basis of morphogenesis. *Nat. Rev. Mol. Cell Biol.* **2011**, *12*, 392–398.
- (3) Brugués, A.; Anon, E.; Conte, V.; Veldhuis, J. H.; Gupta, M.; Colombelli, J.; Muñoz, J. J.; Brodland, G. W.; Ladoux, B.; Trepast, X. Forces driving epithelial wound healing. *Nat. Phys.* **2014**, *10*, 683–690.
- (4) Petridou, N. I.; Spiró, Z.; Heisenberg, C. P. Multiscale force sensing in development. *Nat. Cell Biol.* **2017**, *19*, 581–588.
- (5) Binnig, G.; Quate, C. F.; Gerber, C. Atomic force microscope. *Phys. Rev. Lett.* **1986**, *56*, 930–933.
- (6) Radmacher, M.; Tillmann, R. W.; Gaub, H. E. Imaging viscoelasticity by force modulation with the atomic force microscope. *Biophys. J.* **1993**, *64*, 735–742.
- (7) Radmacher, M.; Tillmann, R.; Fritz, M.; Gaub, H. From molecules to cells: Imaging soft samples with the atomic force microscope. *Science* **1992**, *257*, 1900–1905.
- (8) Matzke, R.; Jacobson, K.; Radmacher, M. Direct, high-resolution measurement of furrow stiffening during division of adherent cells. *Nat. Cell Biol.* **2001**, *3*, 607–610.
- (9) Iyer, S.; Gaikwad, R. M.; Subba-Rao, V.; Woodworth, C. D.; Sokolov, I. Atomic force microscopy detects differences in the surface brush of normal and cancerous cells. *Nat. Nanotechnol.* **2009**, *4*, 389–393.
- (10) Cross, S. E.; Jin, Y. S.; Rao, J.; Gimzewski, J. K. Nanomechanical analysis of cells from cancer patients. *Nat. Nanotechnol.* **2007**, *2*, 780–783.
- (11) Viani, M. B.; Schäffer, T. E.; Chand, A.; Rief, M.; Gaub, H. E.; Hansma, P. K. Small cantilevers for force spectroscopy of single molecules. *J. Appl. Phys.* **1999**, *86*, 2258–2262.
- (12) Laskowski, P. R.; Pfreundschuh, M.; Stauffer, M.; Ucurum, Z.; Fotiadis, D.; Müller, D. J. High-Resolution Imaging and Multi-parametric Characterization of Native Membranes by Combining Confocal Microscopy and an Atomic Force Microscopy-Based Toolbox. *ACS Nano* **2017**, *11*, 8292–8301.
- (13) Moeendarbary, E.; Valon, L.; Fritzsche, M.; Harris, A. R.; Moulding, D. A.; Thrasher, A. J.; Stride, E.; Mahadevan, L.; Charras, G. T. The cytoplasm of living cells behaves as a poroelastic material. *Nat. Mater.* **2013**, *12*, 253–261.
- (14) Hoh, J. H.; Schoenenberger, C. A. Surface morphology and mechanical properties of MDCK monolayers by atomic force microscopy. *Journal of Cell Science* **1994**, *107*, 1105–1114.
- (15) Rotsch, C.; Braet, F.; Wisse, E.; Radmacher, M. AFM imaging and elasticity measurements on living rat liver macrophages. *Cell Biol. Int.* **1997**, *21*, 685–696.
- (16) Rotsch, C.; Jacobson, K.; Radmacher, M. Dimensional and mechanical dynamics of active and stable edges in motile fibroblasts investigated by using atomic force microscopy. *Proc. Natl. Acad. Sci. U. S. A.* **1999**, *96*, 921–926.
- (17) Rotsch, C.; Radmacher, M. Drug-induced changes of cytoskeletal structure and mechanics in fibroblasts: An atomic force microscopy study. *Biophys. J.* **2000**, *78*, 520–535.
- (18) Blau, C.; Kashef, J.; Franz, C. M. Cadherin-11 promotes neural crest cell spreading by reducing intracellular tension—Mapping adhesion and mechanics in neural crest explants by atomic force microscopy. *Semin. Cell Dev. Biol.* **2018**, *73*, 95–106.

- (19) Domke, J.; Parak, W. J.; George, M.; Gaub, H. E.; Radmacher, M. Mapping the mechanical pulse of single cardiomyocytes with the atomic force microscope. *Eur. Biophys. J.* **1999**, *28*, 179–186.
- (20) Chang, W. T.; Yu, D.; Lai, Y. C.; Lin, K. Y.; Liao, I. Characterization of the mechanodynamic response of cardiomyocytes with atomic force microscopy. *Anal. Chem.* **2013**, *85*, 1395–1400.
- (21) Engler, A. J.; Griffin, M. A.; Sen, S.; Bönnemann, C. G.; Sweeney, H. L.; Discher, D. E. Myotubes differentiate optimally on substrates with tissue-like stiffness: pathological implications for soft or stiff microenvironments. *J. Cell Biol.* **2004**, *166*, 877–887.
- (22) Engler, A. J.; Sen, S.; Sweeney, H. L.; Discher, D. E. Matrix Elasticity Directs Stem Cell Lineage Specification. *Cell* **2006**, *126*, 677–689.
- (23) Liu, L.; You, Z.; Yu, H.; Zhou, L.; Zhao, H.; Yan, X.; Li, D.; Wang, B.; Zhu, L.; Xu, Y.; Xia, T.; Shi, Y.; Huang, C.; Hou, W.; Du, Y. Mechanotransduction-modulated fibrotic microniches reveal the contribution of angiogenesis in liver fibrosis. *Nat. Mater.* **2017**, *16*, 1252–1261.
- (24) Odermatt, P. D.; Hannebelle, M. T. M.; Eskandarian, H. A.; Nievergelt, A. P.; McKinney, J. D.; Fantner, G. E. Overlapping and essential roles for molecular and mechanical mechanisms in mycobacterial cell division. *Nat. Phys.* **2020**, *16*, 57–62.
- (25) Saar Dover, R.; Bitler, A.; Shimoni, E.; Trieu-Cuot, P.; Shai, Y. Multiparametric AFM reveals turgor-responsive net-like peptidoglycan architecture in live streptococci. *Nat. Commun.* **2015**, *6*, 1–10.
- (26) Herman-Bausier, P.; Valotteau, C.; Pietrocola, G.; Rindi, S.; Alsteens, D.; Foster, T. J.; Speziale, P.; Dufrière, Y. F. Mechanical Strength and Inhibition of the Staphylococcus aureus. *mBio* **2016**, *7*, 1–11.
- (27) Mohammed, D.; Versaevel, M.; Bruyère, C.; Alaimo, L.; Luciano, M.; Vercruysse, E.; Procès, A.; Gabriele, S. Innovative tools for mechanobiology: Unraveling outside-in and inside-out mechanotransduction. *Front. Bioeng. Biotechnol.* **2019**, *7*, 162.
- (28) O'Shea, C.; Holmes, A. P.; Winter, J.; Correia, J.; Ou, X.; Dong, R.; He, S.; Kirchhof, P.; Fabritz, L.; Rajpoot, K.; Pavlovic, D. Cardiac optogenetics and optical mapping – Overcoming spectral congestion in all-optical cardiac electrophysiology. *Front. Physiol.* **2019**, *10*, 182.
- (29) Caluori, G.; Pribyl, J.; Cmiel, V.; Pesl, M.; Potocnak, T.; Provaznik, I.; Skladal, P.; Rotrekl, V. Simultaneous study of mechanobiology and calcium dynamics on hESC-derived cardiomyocytes clusters. *J. Mol. Recognit.* **2019**, *32*, No. e2760.
- (30) Gaub, B. M.; Müller, D. J. Mechanical Stimulation of Piezo1 Receptors Depends on Extracellular Matrix Proteins and Directionality of Force. *Nano Lett.* **2017**, *17*, 2064–2072.
- (31) Rohr, S.; Salzberg, B. M. Multiple site optical recording of transmembrane voltage (MSORTV) in patterned growth heart cell cultures: assessing electrical behavior, with microsecond resolution, on a cellular and subcellular scale. *Biophys. J.* **1994**, *67*, 1301–1315.
- (32) Cogollo, J. F. S.; Tedesco, M.; Martinoia, S.; Raiteri, R. A new integrated system combining atomic force microscopy and micro-electrode array for measuring the mechanical properties of living cardiac myocytes. *Biomed. Microdevices* **2011**, *13*, 613–621.
- (33) Tian, J.; Tu, C.; Huang, B.; Liang, Y.; Zhou, J.; Ye, X. Study of the union method of microelectrode array and AFM for the recording of electromechanical activities in living cardiomyocytes. *Eur. Biophys. J.* **2017**, *46*, 495–507.
- (34) Upadhye, K. V.; Candiello, J. E.; Davidson, L. A.; Lin, H. Whole-cell electrical activity under direct mechanical stimulus by AFM cantilever using planar patch clamp chip approach. *Cell. Mol. Bioeng.* **2011**, *4*, 270–280.
- (35) Pamir, E.; George, M.; Fertig, N.; Benoit, M. Planar patch-clamp force microscopy on living cells. *Ultramicroscopy* **2008**, *108*, 552–557.
- (36) Meister, A.; Gabi, M.; Behr, P.; Studer, P.; Vörös, J.; Niedermann, P.; Bitterli, J.; Polesel-Maris, J.; Liley, M.; Heinzlmann, H.; Zambelli, T. FluidFM: Combining atomic force microscopy and nanofluidics in a universal liquid delivery system for single cell applications and beyond. *Nano Lett.* **2009**, *9*, 2501–2507.
- (37) Guillaume-Gentil, O.; Potthoff, E.; Ossola, D.; Franz, C. M.; Zambelli, T.; Vorholt, J. A. Force-controlled manipulation of single cells: From AFM to FluidFM. *Trends Biotechnol.* **2014**, *32*, 381–388.
- (38) Ossola, D.; Amarouch, M.-Y.; Behr, P.; Vo Ro S, J.; Abriel, H.; Zambelli, T. Force-Controlled Patch Clamp of Beating Cardiac Cells. *Nano Lett.* **2015**, *15*, 1743–1750.
- (39) Linley, J. E. Perforated whole-cell patch-clamp recording. *Methods Mol. Biol.* **2013**, *998*, 149–157.
- (40) Desbiolles, B. X. E.; De Coulon, E.; Bertsch, A.; Rohr, S.; Renaud, P. Intracellular Recording of Cardiomyocyte Action Potentials with Nanopatterned Volcano-Shaped Microelectrode Arrays. *Nano Lett.* **2019**, *19*, 6173–6181.
- (41) Almquist, B. D.; Melosh, N. A. Fusion of biomimetic stealth probes into lipid bilayer cores. *Proc. Natl. Acad. Sci. U. S. A.* **2010**, *107*, 5815–5820.
- (42) Almquist, B. D.; Verma, P.; Cai, W.; Melosh, N. A. Nanoscale patterning controls inorganic-membrane interface structure. *Nanoscale* **2011**, *3*, 391–400.
- (43) Almquist, B. D.; Melosh, N. A. Molecular structure influences the stability of membrane penetrating biointerfaces. *Nano Lett.* **2011**, *11*, 2066–2070.
- (44) Verma, P.; Melosh, N. A. Gigaohm resistance membrane seals with stealth probe electrodes. *Appl. Phys. Lett.* **2010**, *97*, 033704.
- (45) VanDersarl, J. J.; Renaud, P. Biomimetic surface patterning for long-term transmembrane access. *Sci. Rep.* **2016**, *6*, 32485.
- (46) Hansma, P. K.; Drake, B.; Grigg, D.; Prater, C. B.; Yashar, F.; Gurley, G.; Elings, V.; Feinstein, S.; Lal, R. A new, optical-lever based atomic force microscope. *J. Appl. Phys.* **1994**, *76*, 796–799.
- (47) Desbiolles, B. X. E.; Bertsch, A.; Renaud, P. Ion beam etching redeposition for 3D multimaterial nanostructure manufacturing. *Microsystems & Nanoengineering* **2019**, *5*, 11.
- (48) Huebsch, N.; Loskill, P.; Mandegar, M. A.; Marks, N. C.; Sheehan, A. S.; Ma, Z.; Mathur, A.; Nguyen, T. N.; Yoo, J. C.; Judge, L. M.; Spencer, C. I.; Chukka, A. C.; Russell, C. R.; So, P. L.; Conklin, B. R.; Healy, K. E. Automated video-based analysis of contractility and calcium flux in human-induced pluripotent stem cell-derived cardiomyocytes cultured over different spatial scales. *Tissue Eng., Part C* **2015**, *21*, 467–479.
- (49) Hoang, P.; Jacquir, S.; Lemus, S.; Ma, Z. Quantification of Contractile Dynamic Complexities Exhibited by Human Stem Cell-Derived Cardiomyocytes Using Nonlinear Dimensional Analysis. *Sci. Rep.* **2019**, *9*, 14714.
- (50) Lugstein, A.; Bertagnolli, E.; Kranz, C.; Kueng, A.; Mizaikoff, B. Integrating micro- and nanoelectrodes into atomic force microscopy cantilevers using focused ion beam techniques. *Appl. Phys. Lett.* **2002**, *81*, 349–351.
- (51) Franks, W.; Schenker, I.; Schmutz, P.; Hierlemann, A. Impedance characterization and modeling of electrodes for biomedical applications. *IEEE Trans. Biomed. Eng.* **2005**, *52*, 1295–1302.
- (52) Natarajan, A.; Stancescu, M.; Dhir, V.; Armstrong, C.; Sommerhage, F.; Hickman, J. J.; Molnar, P. Patterned cardiomyocytes on microelectrode arrays as a functional, high information content drug screening platform. *Biomaterials* **2011**, *32*, 4267–4274.
- (53) Shimada, J.; Kaneko, T. Development of Single Cardiomyocyte Measurement of Extracellular Potential. *Biophys. J.* **2016**, *110*, 169a.
- (54) Zhao, Y.; You, S. S.; Zhang, A.; Lee, J.-H.; Huang, J.; Lieber, C. M. Scalable ultrasmall three-dimensional nanowire transistor probes for intracellular recording. *Nat. Nanotechnol.* **2019**, *14*, 783–790.
- (55) Rothe, J.; Frey, O.; Madangopal, R.; Rickus, J.; Hierlemann, A. Robust functionalization of large microelectrode arrays by using pulsed potentiostatic deposition. *Sensors* **2017**, *17*, 22.
- (56) Odermatt, P. D.; Shivanandan, A.; Deschout, H.; Jankele, R.; Nievergelt, A. P.; Feletti, L.; Davidson, M. W.; Radenovic, A.; Fantner, G. E. High-Resolution Correlative Microscopy: Bridging the Gap between Single Molecule Localization Microscopy and Atomic Force Microscopy. *Nano Lett.* **2015**, *15*, 4896–4904.
- (57) Nečas, D.; Klapetek, P. Gwyddion: An open-source software for SPM data analysis. *Central European Journal of Physics* **2012**, *10*, 181–188.